Published for SISSA by Springer

Received: *May 8, 2015*
Revised: *July 28, 2015*
Accepted: *August 20, 2015*
Published: *September 10, 2015*

Cornering dimension-6 HVV interactions at high energy LHC: the role of event ratios

Shankha Banerjee,[a] **Tanumoy Mandal,**[a] **Bruce Mellado**[b] **and Biswarup Mukhopadhyaya**[a]

[a] *Regional Centre for Accelerator-based Particle Physics, Harish-Chandra Research Institute, Chhatnag Road, Jhusi, Allahabad 211019, India*

[b] *School of Physics, University of the Witwatersrand, Johannesburg 2050, South Africa*

E-mail: shankha@hri.res.in, tanumoymandal@hri.res.in, bruce.mellado@wits.ac.za, biswarup@hri.res.in

Abstract: We suggest a way of improving the probes on dimension-6 CP-conserving HVV interactions ($V = W$, Z, γ), from the LHC data on the Higgs boson to be available in the 14 TeV run with an integrated luminosity of 3000 fb^{-1}. We find that the ratios of total rates in different channels can be quite useful in this respect. This includes ratios of event rates in (a) different final states for the Higgs produced by the same production mechanism, and (b) the same final state from two different production modes. While most theoretical uncertainties cancel in the former, the latter helps in the case of those operators which shift the numerator and denominator in opposite directions. Our analysis, incorporating theoretical, systematic and statistical uncertain, leads to projected limits that are better than the strongest ones obtained so far from precision electroweak as well as LHC Higgs data. Moreover, values of the coefficients of the dimension-6 operators, which are allowed in disjoint intervals, can have their ranges narrowed down substantially in our approach.

Keywords: Higgs Physics, Beyond Standard Model

ArXiv ePrint: 1505.00226

doi:10.1007/JHEP09(2015)057

JHEP09(2015)057

Contents

1 Introduction

The ATLAS and CMS experiments at the Large Hadron Collider (LHC) have discovered a neutral spinless particle that closely matches the description of the Higgs boson [1, 2] which is responsible for masses of elementary particles, according to the standard model (SM) of electroweak interactions. While this ties the final knot on the framework embodied in the SM, there are many reasons to believe that there is more fundamental physics at higher energies. The reason for such expectation can be traced to many issues, including the unexplained replication of fermion families, the source of dark matter in the universe, and the problems of naturalness and vacuum stability involving the Higgs boson itself. The Large Hadron Collider (LHC) has not revealed any direct signature of new physics so far. However, one is led to suspect that such physics should affect the interaction Lagrangian of the Higgs boson. This generates, for example, effective operators of dimension-6 contributing to HVV interactions, with $V = W, Z, \gamma$. Probing such effective couplings for the recently discovered scalar is therefore tantamount to opening a gateway to fundamental physics just beyond our present reach.

Such 'effective' interaction terms better be SU(2) × U(1) invariant if they arise from physics above the electroweak scale. Constraints on such terms have already been studied, using precision electroweak data as well as global fits of the current Higgs data [3–37]. Recently, CMS has published an exhaustive study on anomalous HVV couplings [38].

JHEP09(2015)057

Many studies have considered anomalous Higgs couplings in context of future lepton colliders [39–44]. The general conclusion, based on analyses of the 8 TeV data, is that several (though not all) of the gauge invariant, dimension-6 HVV terms have been quite strongly constrained by the EW precision and LHC data (as discussed in section 3) [3–37]. It still remains to be seen whether such small coefficients can be discerned with some ingeniously constructed kinematic distributions. Some work has nonetheless been done to study such distributions [45–49], in terms of either the gauge invariant operators themselves or the structures finally ensuing from them. At the same time, it is of interest to see if meaningful constraints do arise from the study of total rates at the LHC. The essence of any probe of these anomalous couplings, however, lies in pinning them down to much smaller values using the 14 TeV runs, as common sense suggests the manifestation, if any, of new physics through Higher Dimensional Operators (HDO's) with small coefficients only.

We show here that the relative rates of events of different kinds in the Higgs data can allow us to probe such effective interactions to levels of smallness not deemed testable otherwise [50, 51]. This happens through (a) the cancellation of theoretical uncertainties, and (b) the fact that some ratios have the numerators and denominators shifting in opposite directions, driven by the additional interactions. Thus the cherished scheme of finding traces of new physics in Higgs phenomenology can be buttressed with one more brick.

We organise our paper as follows: we summarise the relevant gauge invariant operators and the interaction terms in section 2. In section 3, we introduce three ratios of cross-sections as our observables. The results of our analysis are explained in section 4. We summarise and conclude in section 5.

2 Higher dimensional operators

In order to see any possible deviations from the SM in the Higgs sector, we will follow the effective field theory (EFT) framework. We consider $\mathrm{SU}(2)_L \times \mathrm{U}(1)_Y$ invariant operators of dimension up to 6, which affect Higgs couplings to itself and/or a pair of electroweak vector bosons. While a full list of such operators are found in [52–55], we have concentrated here on dimension-6 CP-conserving operators which affect Higgs phenomenology. They include:

- Operators which contain the Higgs doublet Φ and its derivatives:

$$\mathcal{O}_{\Phi,1} = (D_\mu\Phi)^\dagger\Phi\Phi^\dagger(D^\mu\Phi); \quad \mathcal{O}_{\Phi,2} = \frac{1}{2}\partial_\mu(\Phi^\dagger\Phi)\partial^\mu(\Phi^\dagger\Phi); \quad \mathcal{O}_{\Phi,3} = \frac{1}{3}(\Phi^\dagger\Phi)^3 \tag{2.1}$$

- Those containing Φ (or its derivatives) and the bosonic field strengths:

$$\begin{aligned} &\mathcal{O}_{GG} = \Phi^\dagger\Phi G^a_{\mu\nu}G^{a\,\mu\nu}; && \mathcal{O}_{BW} = \Phi^\dagger\hat{B}_{\mu\nu}\hat{W}^{\mu\nu}\Phi; && \mathcal{O}_{WW} = \Phi^\dagger\hat{W}_{\mu\nu}\hat{W}^{\mu\nu}\Phi \\ &\mathcal{O}_{W} = (D_\mu\Phi)^\dagger\hat{W}^{\mu\nu}(D_\nu\Phi); && \mathcal{O}_{BB} = \Phi^\dagger\hat{B}_{\mu\nu}\hat{B}^{\mu\nu}\Phi; && \mathcal{O}_{B} = (D_\mu\Phi)^\dagger\hat{B}^{\mu\nu}(D_\nu\Phi), \end{aligned} \tag{2.2}$$

where

$$\hat{W}^{\mu\nu} = i\,\frac{g}{2}\sigma_a W^{a\,\mu\nu}; \quad \hat{B}^{\mu\nu} = i\,\frac{g'}{2}B^{\mu\nu}$$

and g, g' are respectively the $\mathrm{SU}(2)_\mathrm{L}$ and $\mathrm{U}(1)_\mathrm{Y}$ gauge couplings. $W^a_{\mu\nu} = \partial_\mu W^a_\nu - \partial_\nu W^a_\mu - g\epsilon^{abc}W^b_\mu W^c_\nu$, $B_{\mu\nu} = \partial_\mu B_\nu - \partial_\nu B_\mu$ and $G^a_{\mu\nu} = \partial_\mu G^a_\nu - \partial_\nu G^a_\mu - g_s f^{abc}G^b_\mu G^c_\nu$. The covariant

JHEP09(2015)057

derivative of Φ is given as $D_\mu\Phi = (\partial_\mu + \frac{i}{2}g'B_\mu + ig\frac{\sigma_a}{2}W^a_\mu)\Phi$. The Lagrangian in the presence of the above operators can be generally expressed as:

$$\mathcal{L} \supset \kappa\left(\frac{2m_W^2}{v}HW^+_\mu W^{\mu-} + \frac{m_Z^2}{v}HZ_\mu Z^\mu\right) + \sum_i \frac{f_i}{\Lambda^2}\mathcal{O}_i, \tag{2.3}$$

where in addition to the dimension-6 (D6) operators, we also allow for the SM-like HWW and HZZ couplings to be scaled by a factor κ. While $\kappa \neq 1$ is indicative of certain kinds of new physics, we are specially interested in this study in the new observable features associated with the HDOs. Therefore, we have set $\kappa = 1$ for simplicity.[1]

No operator of the form $\mathcal{O}_{GG}$ is assumed to exist since we are presently concerned with Higgs interactions with a pair of electroweak vector bosons only. The operator $\mathcal{O}_{\Phi,1}$ is severely constrained by the T-parameter (or equivalently the ρ parameter), as it alters the HZZ and HWW couplings by unequal multiplicative factors. As far as HZZ and HWW interactions are concerned, $\mathcal{O}_{\Phi,2}$ only scales the standard model-like couplings (κ), without bringing in any new Lorentz structure. This amounts to a renormalization of the Higgs field. It also alters the Higgs self-coupling, something that is the sole consequence of $\mathcal{O}_{\Phi,3}$ as well.

In view of the above, we focus on the four operators $\mathcal{O}_{WW}$, $\mathcal{O}_{BB}$, $\mathcal{O}_W$ and $\mathcal{O}_B$. We do not include the operator $\mathcal{O}_{BW} = \Phi^\dagger\hat{B}_{\mu\nu}\hat{W}^{\mu\nu}\Phi$ in the present analysis, because it mixes the Z and γ fields at the tree level, violates custodial symmetry (by contributing only to the Z-boson mass) and is, therefore, highly constrained by the S and T-parameters at the tree level [4]. The effective interactions that finally emerge and affect the Higgs sector are

$$\begin{aligned}\mathcal{L}_{\text{eff}} = {} & g^{(1)}_{HWW}\,(W^+_{\mu\nu}W^{-\mu}\partial^\nu H + h.c.) + g^{(2)}_{HWW}\,HW^+_{\mu\nu}W^{-\mu\nu} \\ & + g^{(1)}_{HZZ}\,Z_{\mu\nu}Z^\mu\partial^\nu H + g^{(2)}_{HZZ}\,HZ_{\mu\nu}Z^{\mu\nu} \\ & + g^{(1)}_{HZ\gamma}\,A_{\mu\nu}Z^\mu\partial^\nu H + g^{(2)}_{HZ\gamma}\,HA_{\mu\nu}Z^{\mu\nu} + g_{H\gamma\gamma}HA_{\mu\nu}A^{\mu\nu},\end{aligned} \tag{2.4}$$

where

$$\begin{aligned} g^{(1)}_{HWW} &= \left(\frac{gM_W}{\Lambda^2}\right)\frac{f_W}{2}; & g^{(2)}_{HWW} &= -\left(\frac{gM_W}{\Lambda^2}\right)f_{WW} \\ g^{(1)}_{HZZ} &= \left(\frac{gM_W}{\Lambda^2}\right)\frac{c^2f_W + s^2f_B}{2c^2}; & g^{(2)}_{HZZ} &= -\left(\frac{gM_W}{\Lambda^2}\right)\frac{s^4f_{BB} + c^4f_{WW}}{2c^2} \\ g^{(1)}_{HZ\gamma} &= \left(\frac{gM_W}{\Lambda^2}\right)\frac{s(f_W - f_B)}{2c}; & g^{(2)}_{HZ\gamma} &= \left(\frac{gM_W}{\Lambda^2}\right)\frac{s(s^2f_{BB} - c^2f_{WW})}{c} \\ g_{H\gamma\gamma} &= -\left(\frac{gM_W}{\Lambda^2}\right)\frac{s^2(f_{BB} + f_{WW})}{2} \end{aligned} \tag{2.5}$$

with $s\,(c)$ being the sine (cosine) of the Weinberg angle. Besides, the operators $\mathcal{O}_W$, $\mathcal{O}_B$ and $\mathcal{O}_{WWW}$ also contribute to the anomalous triple gauge boson interactions which can be summarised as

$$\mathcal{L}_{WWV} = -ig_{WWV}\left\{g_1^V\left(W^+_{\mu\nu}W^{-\mu}V^\nu - W^+_\mu V_\nu W^{-\mu\nu}\right) + \kappa_V W^+_\mu W^-_\nu V^{\mu\nu} + \frac{\lambda_V}{M_W^2}W^+_{\mu\nu}W^{-\nu\rho}V^\mu_\rho\right\}, \tag{2.6}$$

[1] Possible constraints on the departure of κ from unity have been obtained in the literature from global fits of the Higgs data (See for example [3–36]).

JHEP09(2015)057

where $g_{WW\gamma} = g\,s$, $g_{WWZ} = g\,c$, $\kappa_V = 1 + \Delta\kappa_V$ and $g_1^Z = 1 + \Delta g_1^Z$ with

$$\Delta\kappa_\gamma = \frac{M_W^2}{2\Lambda^2}\,(f_W + f_B)\,; \qquad \lambda_\gamma = \lambda_Z = \frac{3g^2 M_W^2}{2\Lambda^2} f_{WWW}$$
$$\Delta g_1^Z = \frac{M_W^2}{2c^2\Lambda^2} f_W; \qquad \Delta\kappa_Z = \frac{M_W^2}{2c^2\Lambda^2}\left(c^2 f_W - s^2 f_B\right) \tag{2.7}$$

The already existing limits on the various operators discussed above are found in numerous references [3–6, 10]. Even within their current limits, some of the operators are found to modify the efficiencies of the various kinetic cuts [9, 14]. The question we address in the rest of the paper is: can these limits be improved in the next run(s) through careful measurement of the ratios of total rates in different channels? As we shall see below, the answer is in the affirmative.

3 Ratios of cross-sections as chosen observables

The four HDOs under consideration affect Higgs production as well as its decays, albeit to various degrees. For example, HDO-dependent single Higgs production processes are in association with vector bosons (VH) i.e. $pp \to VH$ (where $V = \{W, Z\}$) and vector-boson fusion (VBF). We show the production cross-sections in these channels at 14 TeV in figure 1, as functions of the four operator coefficients (f_i) taken one at a time.[2] The relevant decay channels which are dependent on such operators are $H \to WW^*, ZZ^*, \gamma\gamma, Z\gamma$. Figure 2 contains these branching ratios (BR) as functions of the four coefficients under consideration.

The VBF and VH rates are sensitive to f_{WW} and f_W, but depend very weakly on f_{BB} and f_B, while the cross-section $\sigma(pp \to WH)$, is completely independent of f_{BB} and f_B). The HDO effects in $H \to \gamma\gamma$ and $H \to Z\gamma$ for $f_i \sim \mathcal{O}(1)$[3] is of the same order as the loop-induced SM contribution unlike in the case of the HWW and HZZ couplings. Therefore, $\mathrm{BR}_{H\to\gamma\gamma}$ becomes highly sensitive to f_{WW} and f_{BB}. Consequently, the 7+8 TeV data already restrict their magnitudes. Bounds on all these operators in a similar framework can be seen in table VI of ref. [4] and also in ref. [3]. In ref. [4], the bounds have been presented at 90% CL by varying multiple operators at the same time. These bounds have been obtained by considering the LHC data as well as constraints from on the oblique parameters, *viz.*, S, T and U. Bounds coming from the oblique parameters are generally weaker than those obtained from the LHC data as can be seen in ref. [3]. These limits may not be applicable when the analysis is performed varying one operator at a time.

Based on the above information, we set out to find observables which are sensitive to $f_i \lesssim 5\,\mathrm{TeV}^{-2}$ in the High luminosity run at the LHC. It is not completely clear yet how much of statistics is required to probe such small values with various event shape variables. On the other hand, the more straightforward observables, namely, total rates in various

[2] We have used CTEQ6L1 parton distribution functions (PDFs) by setting the factorization (μ_F) and renormalization scales (μ_R) at the Higgs mass ($M_H = 125\,\mathrm{GeV}$).

[3] If the operators arise from loop-induced diagrams which imply 'loop factors' in denominators of the effective interactions, $O(1)\,\mathrm{TeV}^{-2}$ coefficients imply strongly coupled theories [11, 56]. However, if such operators originate from tree-level diagrams, then $O(1)$ TeV^{-2} coefficients imply weakly-coupled theories.

JHEP09(2015)057

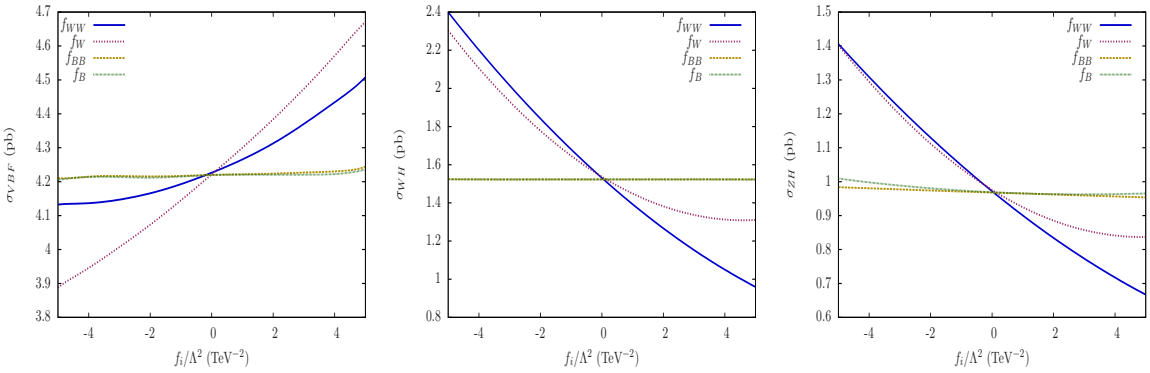

(a) **(b)** **(c)**

Figure 1. Higgs production cross-sections for the VBF and VH channels in presence of HDOs at 14 TeV. Here the operators are varied one at a time.

channels, are also fraught with statistical, systematic and theoretical uncertainties which must be reduced as far as possible when precision is at a premium.

An approach that is helpful is looking at ratios of cross-sections in different channels. In this paper, we invoke two kinds of ratios. First, we take ratios of events in two different final states arising from a Higgs produced via the same channel (in our case, gluon fusion). Such a ratio enables one to get rid of correlated theoretical uncertainties (CThU) such as those in PDF and renormalisation/factorisation scales. They also cancel the uncertainty in total width which is correlated in the calculation of BRs into the two final states. Secondly, we consider the ratio of rates for the same final state for two different production channels (such as VBF and VH). Although the uncertainty in the BR cancels here, the theoretical uncertainties at the production level do not. Moreover, since the final state is same in this case, some systematic uncertainties which are correlated (related to identification, isolation, trigger etc.) will also get cancelled. However, this is helpful in another manner. For some of the operators, the f_i-dependent shifts with respect to the SM are in opposite direction for the numerator and the denominator in such ratios. The result is that the net deviation adds up, as shown in subsection 3.2. We shall see that the use of both these kinds of ratios (including those involving the channel $Z\gamma$ can capture the HDO coefficients at a level unprecedented, going down to values where new physics can show up.

3.1 Observable sensitive to $\mathcal{O}_{WW}$ and $\mathcal{O}_{BB}$: $\mathcal{R}_1$

As has been noted earlier, $\text{BR}_{H\to\gamma\gamma}$ (figure 2c) is highly sensitive to two of the operators, namely, $\mathcal{O}_{BB}$ and $\mathcal{O}_{WW}$. Therefore, we propose to probe them in the $\gamma\gamma$ channel, with the Higgs produced through gluon-gluon fusion (ggF). This final state is clean for reconstruction, and has high statistics. We should mention here that if we consider the simultaneous presence of more than one operators, then there is a "blind-direction" in the parameter space $f_{WW} \approx -f_{BB}$ where $\text{BR}_{H\to\gamma\gamma}$ mimics the SM value. This is because the higher-dimensional part of the $H\gamma\gamma$ vertex is proportional to $f_{WW} + f_{BB}$. Also, for the non-trivial range $f_{WW} = f_{BB} \approx -3$, $\text{BR}_{H\to\gamma\gamma}$ mimics the SM value, due to parabolic

JHEP09(2015)057

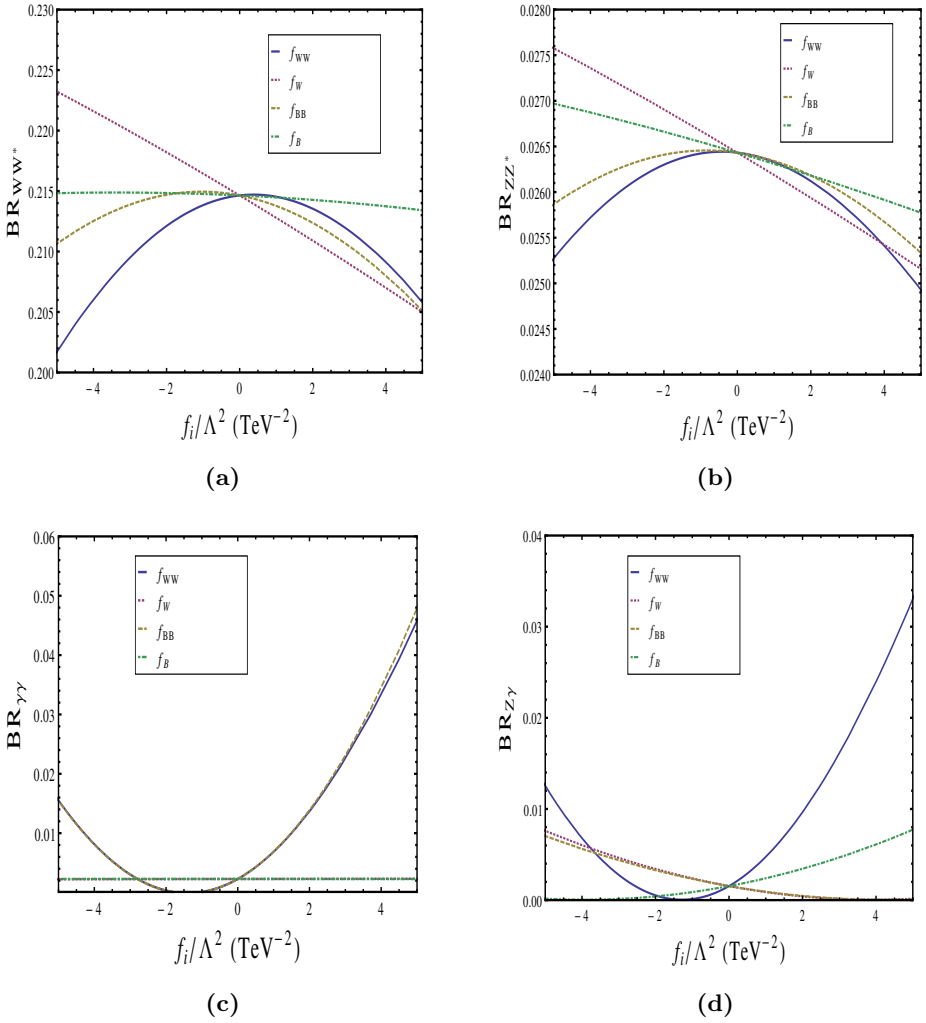

Figure 2. Branching ratios of $H \to WW^*, ZZ^*, \gamma\gamma, Z\gamma$ in presence of HDOs. The operators are varied one at a time.

dependence of the diphoton rate on the HDO coefficients. Therefore, the Higgs produced through ggF followed by its decay to $\gamma\gamma$ cannot be used alone to probe these two 'special' regions of the parameter space. We construct the observable

$$\mathcal{R}_1(f_i) = \frac{\sigma_{\rm ggF} \times {\rm BR}_{H\to\gamma\gamma}(f_i)}{\sigma_{\rm ggF} \times {\rm BR}_{H\to WW^*\to 2\ell 2\nu}(f_i)}, \tag{3.1}$$

where $\ell = e, \mu$ and f_i's are the operator coefficients. As explained earlier, the CThU in production as well as total width cancels here; so does the K-factor in the production rate. Clearly, $\mathcal{R}_1$ can also be expressed as the ratio of two signal strengths as follows,

$$\mathcal{R}_1(f_i) = \frac{\mu^{\rm ggF}_{\gamma\gamma}(f_i)}{\mu^{\rm ggF}_{WW^*}(f_i)} \times \frac{(\sigma_{\rm ggF} \times {\rm BR}_{H\to\gamma\gamma})^{\rm SM}}{(\sigma_{\rm ggF} \times {\rm BR}_{H\to WW^*\to 2\ell 2\nu})^{\rm SM}} \ . \tag{3.2}$$

Therefore, already measured $\gamma\gamma$ and WW^* signal strengths can be used to constrain the operator coefficients affecting the ratio $\mathcal{R}_1$. The efficiency of acceptance cuts does

JHEP09(2015)057

not affect the results, for values of f_{WW} and f_{BB} which are of relevance here because for such small values of the parameter coefficients the change in experimental cut-efficiencies is negligible. On top of that, for the ggF production mode, these operators only affect the decay vertices and hence the cut-efficiencies are but modified by a very small extent. We must also note that in defining $\mathcal{R}_1$ a full jet-veto (0-jet category) has been demanded for both the numerator and the denominator to reduce the uncertainties related to the different jet-requirement in the final state. Besides, in the denominator, the WW^* pair is considered to decay into both same flavour ($ee + \mu\mu$) and different flavour ($e\mu + \mu e$) final states to improve the statistics.

3.2 Observable sensitive to $\mathcal{O}_{WW}$ and $\mathcal{O}_W$: $\mathcal{R}_2$

It turns out that the f_{WW} and f_W affect (to one's advantage) the ratio of events in a particular Higgs decay mode in the VBF and VH channels. This captures the new physics at the production level. By considering the same final states from Higgs decay, some theoretical uncertainties in the decay part cancels out. The production level uncertainties, including the K-factors, however, do not cancel here. In our calculation, the next-to-next-to leading order (NNLO) K-factors have been assumed to be the same as in the SM, expecting that the presence of HDO does not effect the K-factors much. For precise estimate of the observed ratio, one of course has to incorporate the modified cut efficiencies due to the new operators, though such modifications may be small. The other, important advantage in taking the above kind of ratio is that, for not-too-large f_{WW} or f_W (in the range $[-5, +5]$), the deviations of the VBF and VH cross-sections are in opposite directions. The generic deviation for the rate in any channel can be parametrized as

$$\sigma^{\rm HDO}_{\rm prod.} = \sigma^{\rm SM}_{\rm prod.} \times (1 + \delta_{\rm prod.})\,. \tag{3.3}$$

From figure 1a, $\delta_{\rm VBF}$ is positive in the range $f_{WW}, f_W > 0$. On the other hand, in the same region of the parameter space, $\delta_{\rm VH}$ is negative as evident from figures 1b and 1c. Hence, on taking the ratio $\sigma^{\rm HDO}_{\rm VBF}/\sigma^{\rm HDO}_{\rm VH}$, the deviation from SM is

$$\frac{\sigma_{\rm VBF}}{\sigma_{\rm VH}} = \frac{\sigma^{\rm SM}_{\rm VBF}}{\sigma^{\rm SM}_{\rm VH}} \times \left(1 + \delta_{\rm VBF} - \delta_{\rm VH} + \mathcal{O}(\delta^2)\right). \tag{3.4}$$

Thus this ratio further accentuates the deviation from SM behaviour. As an example, if we consider the parameter choice $f_W = 2$, then $\delta_{\rm VBF} \approx 3.6\%$ and $\delta_{\rm WH} \approx 10\%$. However, from the ratio, the combined $\delta_{\rm VBF+WH} \approx 15\%$, which is a clear indication of why we should consider such ratios. We thus define our next observable

$$\mathcal{R}_2(f_i) = \frac{\sigma_{\rm VBF}(f_i) \times {\rm BR}_{H\to\gamma\gamma}(f_i)}{\sigma_{\rm WH}(f_i) \times {\rm BR}_{H\to\gamma\gamma}(f_i) \times {\rm BR}_{W\to\ell\nu}}, \tag{3.5}$$

where the $\gamma\gamma$ final state has been chosen because of its clean character and reconstructibility of the Higgs mass. It should be remembered, however, that f_{WW}, f_{BB} in the range -3 to 0 causes the diphoton branching ratio to undergo a further dip. This can adversely affect the statistics, and thus the high luminosity run is required for an exhaustive scan of the admissible ranges of the above coefficients.

JHEP09(2015)057

3.3 Observable sensitive to $\mathcal{O}_B$: $\mathcal{R}_3$

The operator $\mathcal{O}_B$ is sensitive to $H \to ZZ^*$ and $H \to Z\gamma$. In the former mode, the sensitivity of f_B is limited (see the green curve in figure 2b) and can be appreciable only for larger f_B. The partial decay width $\Gamma_{H\to Z\gamma}$, on the other hand is rather sensitive to all the four operators under study (figure 2d), primarily due to the fact that the new $HZ\gamma$ vertex contributes practically as the same order as in the SM. However, the present statistics in this channel is poor [57, 58]. We expect better bounds on $\mathcal{O}_{WW}$, $\mathcal{O}_{BB}$ and $\mathcal{O}_W$ from the measurements of $\mathcal{R}_1$ and $\mathcal{R}_2$. We use $\mathcal{R}_3$ for the 14 TeV 3000 fb^{-1} run to constrain f_B only, for which other channels fail. In the same spirit as for $\mathcal{R}_1$, we thus define our third observable

$$\mathcal{R}_3(f_i) = \frac{\sigma_{\rm ggF} \times \mathrm{BR}_{H\to Z\gamma\to 2\ell\gamma}(f_i)}{\sigma_{\rm ggF} \times \mathrm{BR}_{H\to WW^*\to 2\ell 2\nu}(f_i)}, \tag{3.6}$$

where $\ell = e, \mu$ and here again the CThU cancels. Here also, we must note that in defining $\mathcal{R}_3$ a full jet-veto has been demanded for both the numerator and the denominator. For the numerator, the Z boson's decay to both an electron pair and a muon pair is considered. Besides, in the denominator, the WW^* pair is taken to decay similar to the $\mathcal{R}_1$ case.

Comparison with the κ-framework: in principle, studies in terms of ratios in different channels can be carried also in the κ-framework [8, 59–61] in which couplings are modified just by scale factors. It should, however, be remembered that the present analysis involves new Lorentz structures and hence brings non-trivial interference terms in the squared amplitudes. Unlike the situation with overall scaling, this prevents the cancellation of the modifying couplings when one considers ratios of events taking (SM+BSM) effects into account.

Even though the ratio $\mathcal{R}_1$ ($\mathcal{R}_3$), dominated by $H\gamma\gamma$ ($HZ\gamma$) vertex, contains no new Lorentz structures, it is still sensitive to the HDOs due to the presence of the HWW vertex in the denominator. Therefore, these ratios, although apparently similar to ratios employing the κ-framework, are different in practice. $\mathcal{R}_2$ is a ratio of σ_{VBF} and σ_{WH} which are sensitive to the operator coefficients as shown in figure 1. In the κ-framework, σ_{VBF} is dominated by the WWH vertex and hence κ_{WW} will approximately cancel in $\mathcal{R}_2$. On the other hand, there will be no trivial cancellations between the numerator and denominator in the HDO-framework.

4 Results of the analysis

For our subsequent collider analysis, the chain we have used is as follows - first we have implemented the relevant dimension-6 interaction terms as shown in eq. (2.4) in FeynRules [62], and generated the Universal FeynRules Output (UFO) [63] model files. These UFO model files have been used in the Monte-Carlo (MC) event generator MadGraph [64] to generate event samples. Next, the parton-showering and hadronisation are performed using Pythia [65] and finally detector level analyses is carried using Delphes [66].

Before we discuss the phenomenological aspects of the aforementioned observables, we re-iterate below the various kinds of uncertainties considered. The two major classes of observables where these uncertainties arise are as follows:

JHEP09(2015)057

SM Quantity	Value	$+ve$ uncert. %	$-ve$ uncert. %
$\mathrm{BR}_{H\to\gamma\gamma}$	2.28×10^{-3}	$+4.99$	-4.89
$\mathrm{BR}_{H\to WW^*}$	2.15×10^{-1}	$+4.26$	-4.20
$\mathrm{BR}_{W\to e\nu_e}$	1.07×10^{-1}	$+0.16$	-0.16
$\mathrm{BR}_{W\to \mu\nu_\mu}$	1.06×10^{-1}	$+0.15$	-0.15
$\mathrm{BR}_{H\to Z\gamma}$	1.54×10^{-3}	$+9.01$	-8.83
$\mathrm{BR}_{Z\to ee}$	3.36×10^{-2}	$+0.004$	-0.004
$\mathrm{BR}_{Z\to \mu\mu}$	3.37×10^{-2}	$+0.007$	-0.007
Total Γ_H	4.07 MeV	$+3.97$	-3.94

Table 1. $\mathrm{BR}_{H\to\gamma\gamma}$, $\mathrm{BR}_{H\to WW^*}$, $\mathrm{BR}_{H\to Z\gamma}$, $\mathrm{BR}_{W\to\ell\nu}$, $\mathrm{BR}_{Z\to\ell\ell}$ and total Higgs width Γ_H (MeV) and their % uncertainties ($+ve$ and $-ve$ refer to positive and negative uncertainties respectively) for a Higgs of mass 125 GeV ($m_W = 80.385$ GeV and $m_Z = 91.1876$ GeV). These numbers are taken from the LHC Higgs Cross section Working Group page [67].

- Same production channel but different final states:
  in such cases (as in $\mathcal{R}_1$ and $\mathcal{R}_3$), the correlated uncertainties lie in PDF+α_s, QCD-scale and in the total Higgs decay width, Γ_H. However, uncertainties in the partial decay widths are uncorrelated.[4] Statistical uncertainties for distinct final states are always uncorrelated and are retained in our analysis. We also assume some systematic uncertainties, whenever shown, to be fully uncorrelated. All surviving uncertainties are added in quadrature to estimate total uncertainties related to our observables.

- Different production channels but same final state:
  for such observables ($\mathcal{R}_2$ in our definition), the only correlated uncertainty is in $\mathrm{BR}_{H\to\gamma\gamma}$. All other uncertainties are uncorrelated and hence are added in quadrature (including the uncertainties in the numerator and the denominator of the ratio $\mathcal{R}_2$). Beside the already mentioned theoretical uncertainties, we also encounter some additional theoretical uncertainty related to the QCD-scale in the WH mode, which we separately discuss in subsection 4.3.

We further assume that the percentage uncertainties remain same even after the inclusion of the anomalous couplings. In order to illustrate, how the uncertainties are taken into consideration, we list the theoretical uncertainties related to relevant Higgs BR and total width in table 1, and related to various production cross-sections in table 2. In table 3, we present the number of surviving events after the selection cuts in the SM at 14 TeV with 3000 fb^{-1} integrated luminosity in the pure production modes. These numbers are taken from refs. [68, 69] except for the $\gamma\gamma$ channel in the VBF production mode, which we estimate by applying a fixed p_T-cut (keeping other cuts are same as in ref. [68]) of 50 GeV

[4] We must mention here that $\Gamma_{H\to\gamma\gamma}$ and $\Gamma_{H\to Z\gamma}$ have tiny correlations with $\Gamma_{H\to WW^*}$ because of the W-boson loop in the former two cases. However, in this present analysis we neglect such small correlations and consider these partial decay widths to be mostly uncorrelated.

JHEP09(2015)057

Process	σ (pb)	+QCD-Scale %	−QCD-Scale %	+(PDF+α_S) %	−(PDF+α_S) %
ggF	49.47	+7.5	−8.0	+7.2	−6.0
VBF	4.233	+0.4	−0.5	+3.3	−3.3
WH	1.522	+0.8	−1.6	+3.2	−3.2
ZH	0.969	+4.0	−3.9	+3.5	−3.5

Table 2. The cross-sections of relevant Higgs production ($m_H = 125\,\text{GeV}$) channels and their QCD-Scale and PDF+α_s uncertainties in %. These numbers are again taken from the LHC Higgs Cross section Working Group page [67].

	$\mathcal{R}_1$	$\mathcal{R}_2$	$\mathcal{R}_3$
N_S^{num}	47724 ($\gamma\gamma$ in ggF)	194 ($\gamma\gamma$ in VBF)	1989 ($Z\gamma$ in ggF)
N_B^{num}	3.16×10^6	1041	691931
N_S^{den}	40850 (WW^* in ggF)	238 ($\gamma\gamma$ in WH)	40850 (WW^* in ggF)
N_B^{den}	366450	995	366450

Table 3. Number of surviving events (taken from refs. [68, 69]) after the selection cuts in the SM at 14 TeV with 3000 fb^{-1} integrated luminosity. These numbers are used to compute the statistical uncertainties (which goes as $\sqrt{N_S + N_B}/N_S$, where N_S and N_B are respectively the number of surviving signal and background events after selection cuts) related to the numerator and denominator of the three observables. Number of events in the VBF ($\gamma\gamma$) channel is computed by applying a fixed p_T-cut (keeping other cuts same as in ref. [68]) of 50 GeV on both the tagged jets instead of η-dependent jet selection cuts as used in the same reference. Number of events for $\gamma\gamma$ in $\mathcal{R}_1$, $Z\gamma$ in $\mathcal{R}_3$ and WW^* for $\mathcal{R}_1$ and $\mathcal{R}_3$ are obtained after putting 0-jet veto and demanding only ggF events. The superscripts *num* and *den* signifies the numerators and denominators of the three observables.

$\mathcal{R}_1$	$\mathcal{R}_2$	$\mathcal{R}_3$
2.87 %	13.83 %	29.63 %

Table 4. Statistical uncertainty for the observables $\mathcal{R}_1$, $\mathcal{R}_2$ and $\mathcal{R}_3$. The numbers are obtained after doubling the number of signal and background events given in table 3 in order to account for both ATLAS and CMS experiments.

	$\mathcal{R}_1$	$\mathcal{R}_2$	$\mathcal{R}_3$
Numerator	2.5% ($\gamma\gamma$ in ggF)	9.1% ($\gamma\gamma$ in VBF)	3.1% ($Z\gamma$ in ggF)
Denominator	3.4% (WW^* in ggF)	5.0% ($\gamma\gamma$ in WH)	2.8% (WW^* in ggF)

Table 5. Systematic uncertainties used in our analysis to compute the total uncertainties related to the three observables. The numbers shown here are combination of various types of relevant systematic uncertainties added in quadrature taken from refs. [57, 70, 71].

JHEP09(2015)057

on both the tagged jets instead of η-dependent jet selection cuts as used in the same reference. The number of events have been computed by removing the contaminations from other production mechanisms which will reduce the number of events and hence enhance the statistical uncertainties (which roughly goes as $\sqrt{N_S + N_B}/N_S$, with N_S and N_B being respectively the number of surviving signal and background events after selection cuts). For instance, the reported number of $\gamma\gamma$ events for an integrated luminosity of 3000 fb^{-1} is 49200 with a 3% contamination from VBF (table 3 in ref. [68]). In our analysis we have used $N_S = 47724$ ($= 0.97 \times 49200$) to compute the statistical uncertainty. Similarly a 30% contamination in the VBF category due to ggF (table 3 in ref. [68]) has also been taken into consideration. In doing so, we are giving conservative estimates on the statistical uncertainties. All entries in table 3 are shown after removing contamination to compute conservative statistical uncertainties. We must note that, while computing the statistical uncertainties (as shown in table 4) for all the three ratios, we double the number of events in table 3 to roughly accommodate two independent experiments to be performed by ATLAS and CMS. Here, we assume that ATLAS and CMS will analyse the same channels with similar set of selection cuts and will roughly obtain same number of events in the actual experiment. It is also assumed that the overall performance of ATLAS and CMS will be similar, integrated over a large luminosity. In future, when the data become actually available, one would be able to compute the exact statistical uncertainties. However, we must note that one should actually take the number of events in the *side-band* ($N_{side-band}$) in order to compute the statistical uncertainties. The procedure we follow gives conservative values for the statistical uncertainties. In future, the actual experiments will provide us $N_{side-band}$ which will allow us to compute accurate statistical uncertainties. However, the *side-band* analysis is beyond the scope of this paper as the data for the 14 TeV run at 3000 fb^{-1} is yet unavailable.

We also use some systematic uncertainties in our analysis as listed in table 5 (refs. [57, 70, 71]). In the future, it is quite expected, various systematic uncertainties will reduce by improving their modelling. To be conservative, we have used various important uncorrelated systematic uncertainties as used in refs. [57, 70, 71] for 7+8 TeV analysis. For the observable $\mathcal{R}_1$, since we are applying same jet veto (i.e. 0-jet category), the systematic uncertainties related to the jet energy scale, jet vertex fraction etc. will not be present. On the other hand, due to the different final state, systematic uncertainties related to the photon and lepton identification and isolation, missing energy trigger etc. will remain. In a similar fashion, for $\mathcal{R}_2$ and $\mathcal{R}_3$ various correlated systematic uncertainties will cancel between their respective numerator and denominator.

Next, we consider the ratio $\mathcal{R}_1$ in the light of both the existing data and those predicted for the high energy run. For $\mathcal{R}_2$ and $\mathcal{R}_3$, only a discussion in terms of 14 TeV rates is relevant, as the currently available results have insufficient statistics on these.

4.1 $\mathcal{R}_1$ @ 7+8 TeV

Before predicting the bounds from the 14 TeV HL run, let us form an idea about the constraints from the 7+8 TeV Higgs data in the $\gamma\gamma$ and WW^* channels. In table 6, we show the *exclusive* signal strengths in the $\gamma\gamma$ and WW^* final states through the ggF production mode as reported by ATLAS [70, 71] and CMS [72, 73].

JHEP09(2015)057

Experiment	$\mu(H \to \gamma\gamma)$ in ggF	$\mu(H \to WW^* \to 2\ell \not{E}_T)$ in ggF
ATLAS (@ 7+8 TeV)	$1.32^{+0.38}_{-0.38}$	$1.02^{+0.29}_{-0.26}$
CMS (@ 7+8 TeV)	$1.12^{+0.37}_{-0.32}$	$0.75^{+0.29}_{-0.23}$
Combined	1.21 ± 0.26	0.88 ± 0.19

Table 6. Measured Higgs Signal strengths in the $\gamma\gamma$ and WW^* modes where Higgs is produced through only ggF channel using $\sqrt{s} = 7 + 8$ TeV data by ATLAS [70, 71] and CMS [60, 72]. Here we have combined the ATLAS and CMS signal strengths for a particular final state and production mode using eq. (4.1).

We must emphasize that the categorization introduced by the ATLAS and CMS experiments are used to enhance the sensitivity for the Higgs boson signal (tables II and III in ref. [70]). The signal strengths (μ) shown in figure 17 include these contaminations. These signal strengths are further combined to give specific production categories as shown in figure 18. For instance μ for *ggF categories* is the combination of the four categories, *viz.* central low P_{T_t}, central high P_{T_t}, forward low P_{T_t} and forward high P_{T_t}. Therefore, the μ for specific categories in figure 18 is not *exclusive*. However, while obtaining the μ for a specific production mode in figure 19, the effect of contaminations are properly removed (by knowing the amount of contaminations from Monte-Carlo simulation for the SM) and therefore, these are the *exclusive* signal strengths. The removal of contaminations includes not only the subtraction of production mechanisms that are not of interest but also the propagation of errors. The experiments have taken into account the impact on the statistical, systematic and theoretical errors for the extraction of the *exclusive* signal strengths. Therefore, the *exclusive* μ will generally contain larger uncertainty. For example one can see that the error on the global signal strength is significantly better than that extracted for individual production mechanisms. For instance, in ref. [70], where ATLAS reports on signal strengths with the di-photon channel, the global signal strength is $\mu = 1.17 \pm 0.27$, which leads to an accuracy of 23%, whereas for the signal strength of gluon-gluon fusion (ggf) $\mu_{ggf} = 1.32 \pm 0.38$, corresponding to an accuracy of 29%. Same applies to the results reported by CMS in ref. [72].

Here we statistically combine the signal strengths for a particular final state as reported by the two experiments, using the following relations

$$\frac{1}{\bar{\sigma}^2} = \sum_i \frac{1}{\sigma_i^2}; \qquad \frac{\bar{\mu}}{\bar{\sigma}^2} = \sum_i \frac{\mu_i}{\sigma_i^2}, \tag{4.1}$$

where $\bar{\sigma}$ ($\bar{\mu}$) refers to the combined 1σ uncertainty (signal strength) and σ_i (μ_i) signifies the corresponding uncertainties (signal strengths) in different experiments.

We compute all the surviving correlated theory errors and subtract them in quadrature from the errors in the numerator and denominator of the ratio $\mathcal{R}_1$, *viz.* $\mathcal{R}_1^{num.} = \mu^{\rm ggF}_{H\to\gamma\gamma} \times (\sigma_{\rm ggF} \times {\rm BR}_{H\to\gamma\gamma})^{\rm SM}$ and $\mathcal{R}_1^{den.} = \mu^{\rm ggF}_{H\to WW^*} \times (\sigma_{\rm ggF} \times {\rm BR}_{H\to WW^*})^{\rm SM} \times \sum_\ell {\rm BR}^2_{W\to\ell\nu_\ell}$.[5] In figure 3, the red line is the theoretically computed $\mathcal{R}_1$ which is independent of the centre

[5]For instance, the error associated with combined (ATLAS+CMS) $\mu^{ggF}(H \to \gamma\gamma)$ i.e. ± 0.26 consists of

JHEP09(2015)057

of mass energy since $\mathcal{R}_1$ is actually a ratio of two BRs. The outer (light green) band shows the uncertainty comprising of the uncorrelated theoretical, statistical and systematic parts and the inner (dark green) band represents the total uncorrelated theory uncertainty. The black dashed line gives the experimental central value of $\mathcal{R}_1$. The ratio, $\mathcal{R}_1$ is almost completely dominated by $\mathrm{BR}_{H\to\gamma\gamma}$ (since $\mathrm{BR}_{H\to WW^*}$ is not so sensitive on HDOs) and therefore highly sensitive to the operators $\mathcal{O}_{WW}$ and $\mathcal{O}_{BB}$. The parabolic nature of the $\mathrm{BR}_{H\to\gamma\gamma}$ as functions of f_{WW} and f_{BB} leads to two disjoint allowed ranges of $f_{WW} = f_{BB} \approx [-3.32, -2.91] \cup [0.12, 0.57]$ as shown in figure 3. We should mention that the region between these two allowed ranges shows extremely low values of $\mathrm{BR}_{H\to\gamma\gamma}$ because of destructive interference between the SM and HDO might leads to poor statistics. If both $\mathcal{O}_{WW}$ and $\mathcal{O}_{BB}$ are present simultaneously with almost equal magnitude and opposite signs, the observable $\mathcal{R}_1$ closely mimics the SM expectation, and to probe that 'special' region of parameter space we need to go for other observable like $\mathcal{R}_2$. The operators $\mathcal{O}_W$ and $\mathcal{O}_B$ are mostly insensitive to this observable mainly because $\mathrm{BR}_{\gamma\gamma}$ is independent of these operators and the dependence of BR_{WW^*} on all four operators is comparatively weak (see figure 2a)

We compare our results with the existing bounds on these operators as obtained in literature. For instance, the limits obtained in figure 3 (left panel) of ref. [3] on $\mathcal{O}_{WW}$ and $\mathcal{O}_{BB}$ at 68% CL are $[-3.23, -2.61] \cup [-0.35, 0.27]$ (in TeV^{-2}) for the ATLAS case. In obtaining these limits, they varied one operator at a time. This is similar in approach to our study where we have given a framework where one operator is varied at a time. Our bounds are in very good agreement with their results. The slightly different limits obtained by us are due to the use of more recent data in our case.

4.2 $\mathcal{R}_1$ @ 14 TeV

Next, we present a projected study of $\mathcal{R}_1$ for the 14 TeV run at $3000\,\mathrm{fb}^{-1}$ of integrated luminosity. It should be noted here that the systematic uncertainties used here are for the 8 TeV run and we have assumed that they will not change significantly for the HL-LHC at 14 TeV. The inner bands, more clearly noticeable in figure 4b, contain only the uncorrelated theoretical errors, while the statistical and systematic errors are compounded in the outer bands. Clearly, the uncertainty gets reduced, as compared to $\mathcal{R}_1$ (@ 7 + 8 TeV), and we get an even smaller window around f_{WW} and $f_{BB} \approx [-2.76, -2.65] \cup [-0.06, 0.04]\,\mathrm{TeV}^{-2}$ as shown in figure 4. The difference in this case is that the projected band is around the SM in contrast to what was shown for the 7+8 TeV case, where the ratio of the experimental signal strengths was treated as the reference.

4.3 $\mathcal{R}_2$ @ 14 TeV

We now show the potential of $\mathcal{R}_2$ in deriving bounds on some of the operator coefficients at 14 TeV. As is evident from eq. (3.5), this ratio has the capacity to probe $\mathcal{O}_W$ which cannot be constrained from $\mathcal{R}_1$. On the other hand, the operator $\mathcal{O}_{BB}$, though amenable to probe via $\mathcal{R}_1$, fails to show any marked effect on $\mathcal{R}_2$ because $\mathrm{BR}_{H\to\gamma\gamma}$ gets cancelled in

theoretical, statistical and systematic uncertainties and, by subtracting the CThU (± 0.13) in quadrature we get (± 0.22) which will finally contribute to the uncertainty related to the numerator of $\mathcal{R}_1$.

JHEP09(2015)057

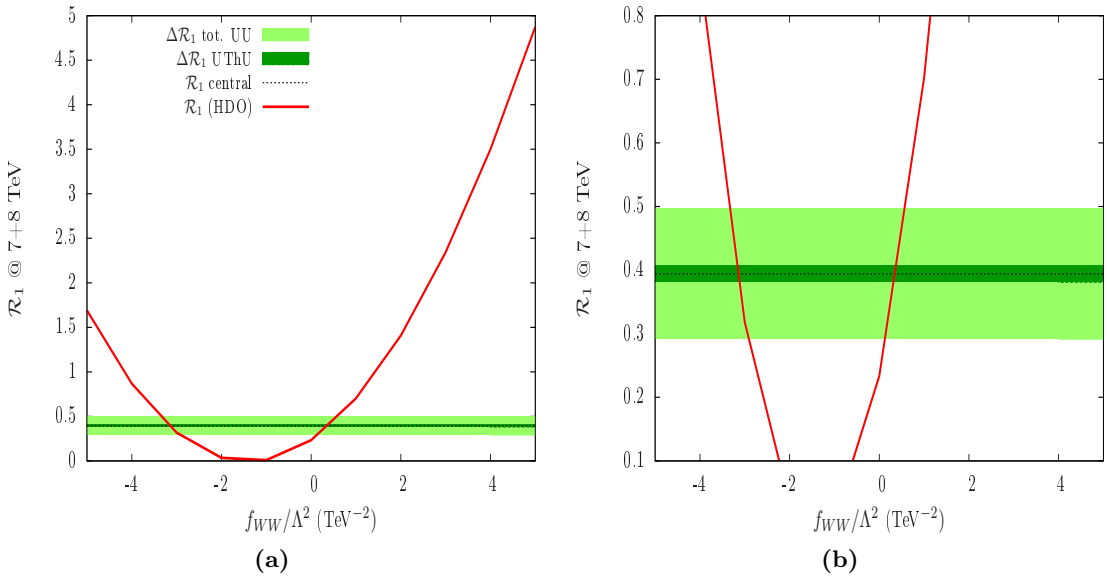

Figure 3. (a) $\mathcal{R}_1$ versus f_{WW}/Λ^2 (TeV^{-2}) and (b) same plot in magnified scale. Plots (a) and (b) are identical for f_{BB}/Λ^2. The red line is the theoretical expectation in presence of HDOs. The inner band (dark green) shows the uncorrelated theoretical uncertainty (UThU) and the outer (light green) band shows the total surviving uncorrelated uncertainty (UU) (uncorrelated theoretical + statistical + systematic) at 7+8 TeV computed using the $\mu_{\gamma\gamma}$ and μ_{WW^*} (CMS+ATLAS) results. The black dotted line is the corresponding central value. The uncertainty bands correspond to 68% CL.

the ratio as defined by us. Also, $\mathcal{O}_{BB}$ does not modify $\sigma_{\rm WH}$ but, $\mathcal{R}_2$ is however sensitive to the operator $\mathcal{O}_{WW}$ as both $\sigma_{\rm VBF}$ and $\sigma_{\rm WH}$ are sensitive to this.

By closely following the ATLAS analyses in the context of high luminosity LHC run, we have used a trigger cut of 50 GeV on jet p_T, instead of using η-dependent p_T cut for jets as used in ref. [68]. The reason is that, a flat cut on the p_T will most certainly give us a less pessimistic number of final state events than that for the η dependent p_T cuts and performs as good as the η-dependent cut to suppress the background. So, we estimate a slightly larger number of events, i.e. we obtain a better efficiency to the cuts for the flat p_T case as compared to what is predicted by ATLAS. For the WH production mode, we use a matched sample with $WH + 0, 1, 2$ jets with the W decaying leptonically. Finally we demand samples with a maximum of one jet in our analysis. In selecting this $0 + 1$ jet sample, from a matched two jet sample, we encounter another theoretical scale uncertainty as described in ref. [74]. We have estimated this uncertainty as follows:

$$\Delta^{th.} = \left.\frac{\sigma(pp \to WH + \geq 2\,\text{jets})}{\sigma^{NNLO}(pp \to WH)}\right|_{m_H} \times \Delta\sigma(pp \to WH + \geq 2\,\text{jets})(\mu_F, \mu_R), \tag{4.2}$$

where $\Delta\sigma(pp \to WH + \geq 2\,\text{jets})$ is the maximum deviation of the exclusive 2-jet cross-section computed at $\mu_F = \mu_R = m_H$ from the ones computed by varying μ_F and μ_R between $m_H/2$ and $2m_H$.

JHEP09(2015)057

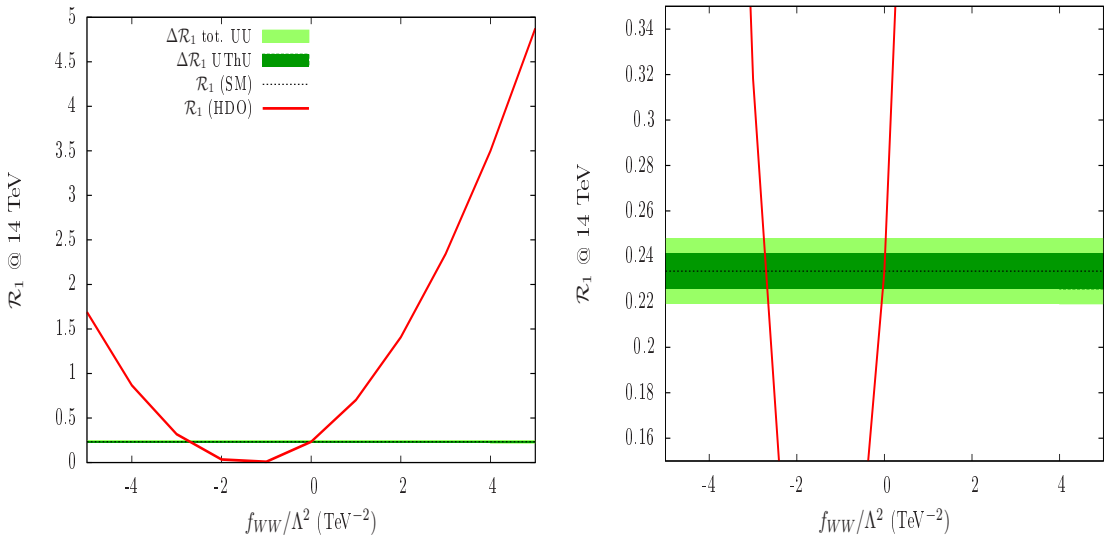

Figure 4. (a) $\mathcal{R}_1$ versus f_{WW}/Λ^2 (TeV^{-2}) and (b) same plot in magnified scale. Plots (a) and (b) are identical for f_{BB}/Λ^2. The red line is the theoretical expectation in presence of HDOs. The inner band (dark green) shows the uncorrelated theoretical uncertainty (UThU) and the outer band (light green) shows total uncorrelated uncertainty (UU) (uncorrelated theoretical + statistical + systematic) at 14 TeV with 3000 fb^{-1} integrated luminosity. The black dotted line is the corresponding central value. The uncertainty bands correspond to 68% CL.

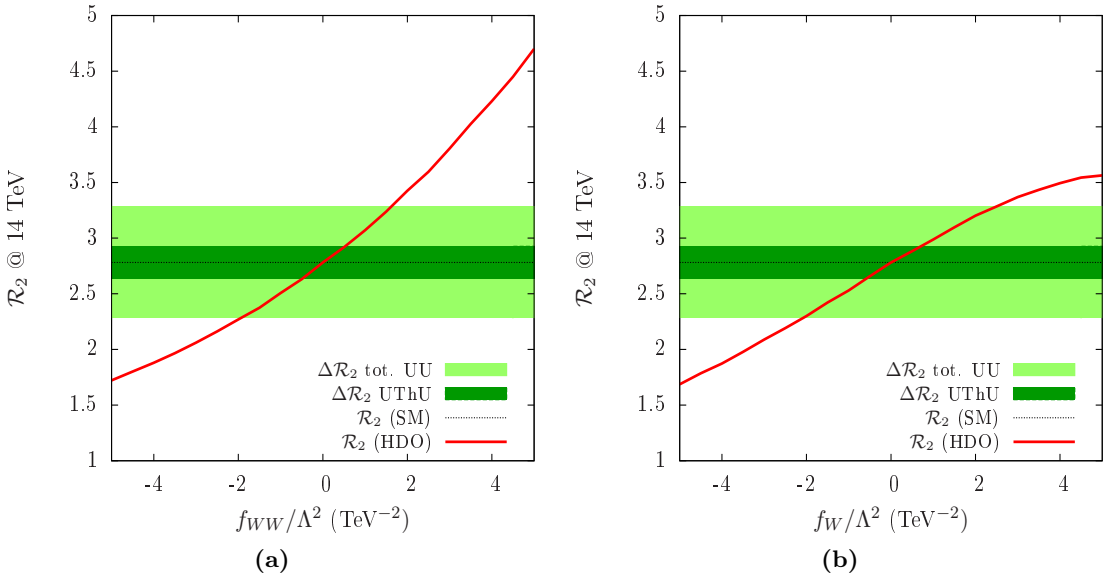

Figure 5. The ratio $\mathcal{R}_2$ versus (a) f_{WW}/Λ^2 (TeV^{-2}), (b) f_W/Λ^2 (TeV^{-2}) for the 14 TeV analysis with 3000 fb^{-1}. The red line is the theoretical expectation in presence of HDOs. The inner band (dark green) shows the uncorrelated theoretical uncertainty due to PDF+α_s, QCD-scale and $\Delta^{th.}$ which is defined in eq. (4.2). The outer band (light green) shows the uncertainties due to the statistical, systematic compounded with the uncorrelated theoretical part. The black dotted line is the corresponding SM value. The uncertainty bands correspond to 68% CL.

JHEP09(2015)057

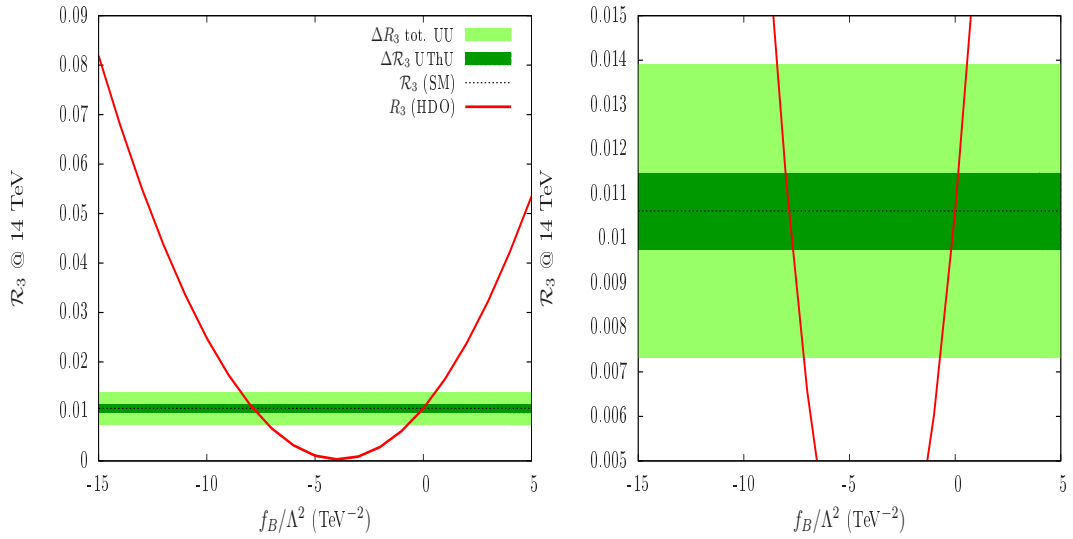

Figure 6. The ratio $\mathcal{R}_3$ versus f_B/Λ^2 (TeV^{-2}) at 14 TeV with 3000 fb^{-1}. The red line is the theoretical expectation in presence of HDOs. The inner band (dark green) shows the uncorrelated theoretical uncertainty (UThU) and the outer band (light green) shows the total uncorrelated uncertainty (UU) due to statistical, systematic and the uncorrelated theoretical part. These uncertainty bands are for $\mathcal{R}_3$ at 14 TeV. The black dotted line is the corresponding SM value. The uncertainty bands correspond to 68% CL.

In constructing $\mathcal{R}_2$, we include the modified cut-efficiencies [9, 14] for both the VBF and WH channels. Even though we stick to small values of f_i where the modification in such efficiencies from the SM-values are small, we still incorporate these to make the study more rigorous. In computing the statistical uncertainties, we took the relevant numbers from the 14 TeV projected study done by ATLAS (see refs. [68, 69]). Besides, we also suggest tagging a single jet for VBF, which reduces the statistical uncertainty by a factor of $\sqrt{2}$ [75]. The $\sqrt{2}$ factor takes into account the number of events as well as the contamination due to ggF as can be seen on table 1 in ref. [75]. In figure 5, we present $\mathcal{R}_2$ as a function of the f_{WW} and f_W taken one at a time for an integrated luminosity of $\mathcal{L} = 3000\,\text{fb}^{-1}$. The outer band (light green) shows the uncertainties due to the statistical, systematic compounded with the uncorrelated theoretical part. The central black dashed line shows the SM expectation for $\mathcal{R}_2$. We can see in figure 5 that very small values of HDO coefficients can be probed by measuring the observable $\mathcal{R}_2$. For f_{WW}, one can corner the allowed region to a small window of $[-1.96, +1.62]$ and for f_W the range would be $[-2.10, +2.50]$. Predicting the observability of such small values in the parameter coefficients is definitely an improvement on existing knowledge.

4.4 $\mathcal{R}_3$ @ 14 TeV

The operator $\mathcal{O}_B$ appears only in the HZZ and $HZ\gamma$ couplings, As seen in figure 2b, the sensitivity of $\mathcal{O}_B$ is too low and hence $H \to ZZ^*$ will not give a proper bound on f_B/Λ^2.

JHEP09(2015)057

Observable	$\mathcal{O}_{WW}$	$\mathcal{O}_{BB}$	$\mathcal{O}_{W}$	$\mathcal{O}_{B}$
$\mathcal{R}_1$ @ 7+8 TeV	$[-3.32, -2.91]$ $\cup$ $[+0.12, +0.57]$	$[-3.32, -2.91]$ $\cup$ $[+0.12, +0.57]$	Not bounded	Not bounded
$\mathcal{R}_1$ @ 14 TeV	$[-2.76, -2.65]$ $\cup$ $[-0.06, +0.04]$	$[-2.76, -2.65]$ $\cup$ $[-0.06, +0.04]$	Not bounded	Not bounded
$\mathcal{R}_2$ @ 14 TeV	$[-1.96, +1.62]$	Not bounded	$[-2.10, +2.50]$	Not bounded
$\mathcal{R}_3$ @ 14 TeV	Not used	Not used	Not used	$[-8.44, -7.17]$ $\cup$ $[-0.72, +0.56]$

Table 7. We summarize our obtained allowed region of the coefficients of HDOs using the three observables. $\mathcal{R}_3$ is not used to constrain the operators $\mathcal{O}_{WW}, \mathcal{O}_{BB}$ and $\mathcal{O}_W$ as has been discussed in section 3.3.

Recent experiment by ATLAS (CMS) puts bounds on the observed signal strength of $H \to Z\gamma$ at about 11 (9.5) times the SM expectation at 95% confidence level [57, 58]. Instead of using these weak signal strengths, we perform an analogous projected study of $\mathcal{R}_3$ at 14 TeV in the same spirit as $\mathcal{R}_1$ at 14 TeV. From figure 6, we find that the projected bounds on f_B/Λ^2 is $[-8.44, -7.17] \cup [-0.72, +0.56]$. The region in between is again inaccessible due to poor statistics, as in this region, $\text{BR}_{H\to Z\gamma}$ becomes insignificant, the reasons being similar to those mentioned for $H \to \gamma\gamma$. The inner band (dark green) includes the uncorrelated theoretical uncertainties due to the partial decay widths of $H \to Z\gamma$ and $H \to WW^*$. The outer band (light green), in addition to the theoretical uncertainties, contains the statistical and systematic uncertainties. As discussed earlier, a few types of correlated systematic uncertainties related to the uncertainty in luminosity, lepton identification and isolation etc. will get cancelled in the ratio $\mathcal{R}_3$. On the other hand, photon identification, isolation etc. uncertainties will retain in the analysis. In table 7, we summarize our obtained region of the parameter space allowed using three ratios, $\mathcal{R}_1$, $\mathcal{R}_2$ and $\mathcal{R}_3$. We present $\mathcal{R}_1$ using combined ATLAS+CMS data for 7+8 TeV run. We also present a projected study for all three observables at 14 TeV with an integrated luminosity of 3000 fb^{-1}. The allowed regions on f_{WW} and f_{BB} shrink at the 14 TeV 3000 fb^{-1} run as compared to the current data. Using the ratio, $\mathcal{R}_2$ one can also put bounds on f_{WW} and f_W. As mentioned earlier, there is a 'special' region of parameter space where $\mathcal{R}_1$ mimics the SM expectation, therefore, $\mathcal{R}_2$ can also be used to infer the presence of $\mathcal{O}_{WW}$ with 'special' values of coefficient f_{WW}. The operator $\mathcal{O}_B$ does not show any appreciable sensitivity in any production of Higgs or its decay except in the $\text{BR}_{H\to Z\gamma}$. Therefore, the ratio $\mathcal{R}_3$ is constructed to constrain f_B by a significant amount as evident from table 7.

JHEP09(2015)057

5 Summary and conclusions

We have investigated how well one can constrain dimension-6 gauge-invariant operators inducing anomalous HVV interactions. Probing the gauge invariant operators individually, we feel, are important, since they can point at any new physics above the electroweak symmetry breaking scale. While the operators contributing to $H \to \gamma\gamma$ are subjected to the hitherto strongest limits using the (7+8) TeV data, the remaining ones are relatively loosely constrained, in spite of the bounds coming from precision electroweak observables. At any rate, it is necessary to reduce uncertainties as much as possible, since any realistically conceived new physics is likely to generate such operators with coefficients no greater than $\approx \mathcal{O}(1)\,\text{TeV}^{-2}$. We show that a good opportunity to probe them at this level, and improve spectacularly over the existing constraints, arises if event ratios in various channels are carefully studied. These include both ratios of events in different final states with the same Higgs production channel and those where a Higgs produced by different production modes ends up decaying into the same final state. While a majority of the theoretical uncertainties cancel in the former category, the latter allow us to probe those cases where some dimension-6 operators shift the rates in the numerator and the denominator in opposite directions. We find that, after a thorough consideration of all uncertainties, all the couplings can be pinned down to intervals of width $\approx \mathcal{O}(1)\,\text{TeV}^{-2}$ on using $3000\,\text{fb}^{-1}$ of integrated luminosity at 14 TeV. Even with 300 fb^{-1}, the improvement over existing constraints is clearly expected, and the results are more uncertainty-free than in any other hitherto applied method. However, we must mention here that this approach should be complemented with the study of differential distributions which is not within the scope of this paper.

Acknowledgments

The work of S.B., T.M. and B. Mukhopadhyaya was partially supported by funding available from the Department of Atomic Energy, Government of India for the Regional Centre for Accelerator-based Particle Physics (RECAPP), Harish-Chandra Research Institute. B. Mellado acknowledges the hospitality of RECAPP, Harish-Chandra Research Institute, during the collaboration.

References

[1] ATLAS collaboration, *Observation of a new particle in the search for the standard model Higgs boson with the ATLAS detector at the LHC*, *Phys. Lett.* **B 716** (2012) 1 [arXiv:1207.7214] [INSPIRE].

[2] CMS collaboration, *Observation of a new boson at a mass of* 125 *GeV with the CMS experiment at the LHC*, *Phys. Lett.* **B 716** (2012) 30 [arXiv:1207.7235] [INSPIRE].

JHEP09(2015)057

[3] E. Massó and V. Sanz, *Limits on anomalous couplings of the Higgs boson to electroweak gauge bosons from LEP and the LHC*, *Phys. Rev.* **D 87** (2013) 033001 [arXiv:1211.1320] [INSPIRE].

[4] T. Corbett, O.J.P. Éboli, J. Gonzalez-Fraile and M.C. Gonzalez-Garcia, *Robust determination of the Higgs couplings: power to the data*, *Phys. Rev.* **D 87** (2013) 015022 [arXiv:1211.4580] [INSPIRE].

[5] A. Falkowski, F. Riva and A. Urbano, *Higgs at last*, *JHEP* **11** (2013) 111 [arXiv:1303.1812] [INSPIRE].

[6] T. Corbett, O.J.P. Éboli, J. Gonzalez-Fraile and M.C. Gonzalez-Garcia, *Determining triple gauge boson couplings from Higgs data*, *Phys. Rev. Lett.* **111** (2013) 011801 [arXiv:1304.1151] [INSPIRE].

[7] B. Dumont, S. Fichet and G. von Gersdorff, *A Bayesian view of the Higgs sector with higher dimensional operators*, *JHEP* **07** (2013) 065 [arXiv:1304.3369] [INSPIRE].

[8] S. Banerjee, S. Mukhopadhyay and B. Mukhopadhyaya, *New Higgs interactions and recent data from the LHC and the Tevatron*, *JHEP* **10** (2012) 062 [arXiv:1207.3588] [INSPIRE].

[9] J.S. Gainer, J. Lykken, K.T. Matchev, S. Mrenna and M. Park, *Geolocating the Higgs boson candidate at the LHC*, *Phys. Rev. Lett.* **111** (2013) 041801 [arXiv:1304.4936] [INSPIRE].

[10] T. Corbett, O.J.P. Éboli, J. Gonzalez-Fraile and M.C. Gonzalez-Garcia, *Robust determination of the scalar boson couplings*, arXiv:1306.0006 [INSPIRE].

[11] J. Elias-Miro, J.R. Espinosa, E. Masso and A. Pomarol, *Higgs windows to new physics through $D = 6$ operators: constraints and one-loop anomalous dimensions*, *JHEP* **11** (2013) 066 [arXiv:1308.1879] [INSPIRE].

[12] A. Pomarol and F. Riva, *Towards the ultimate SM fit to close in on Higgs physics*, *JHEP* **01** (2014) 151 [arXiv:1308.2803] [INSPIRE].

[13] M.B. Einhorn and J. Wudka, *Higgs-boson couplings beyond the standard model*, *Nucl. Phys.* **B 877** (2013) 792 [arXiv:1308.2255] [INSPIRE].

[14] S. Banerjee, S. Mukhopadhyay and B. Mukhopadhyaya, *Higher dimensional operators and the LHC Higgs data: the role of modified kinematics*, *Phys. Rev.* **D 89** (2014) 053010 [arXiv:1308.4860] [INSPIRE].

[15] S. Willenbrock and C. Zhang, *Effective field theory beyond the standard model*, *Ann. Rev. Nucl. Part. Sci.* **64** (2014) 83 [arXiv:1401.0470] [INSPIRE].

[16] J. Ellis, V. Sanz and T. You, *Complete Higgs sector constraints on dimension-6 operators*, *JHEP* **07** (2014) 036 [arXiv:1404.3667] [INSPIRE].

[17] H. Belusca-Maito, *Effective Higgs Lagrangian and constraints on Higgs couplings*, arXiv:1404.5343 [INSPIRE].

[18] R.S. Gupta, A. Pomarol and F. Riva, *BSM primary effects*, *Phys. Rev.* **D 91** (2015) 035001 [arXiv:1405.0181] [INSPIRE].

[19] E. Masso, *An effective guide to beyond the standard model physics*, *JHEP* **10** (2014) 128 [arXiv:1406.6376] [INSPIRE].

[20] A. Biekötter, A. Knochel, M. Krämer, D. Liu and F. Riva, *Vices and virtues of Higgs effective field theories at large energy*, *Phys. Rev.* **D 91** (2015) 055029 [arXiv:1406.7320] [INSPIRE].

[21] C. Englert and M. Spannowsky, *Effective theories and measurements at colliders*, *Phys. Lett.* **B 740** (2015) 8 [arXiv:1408.5147] [INSPIRE].

JHEP09(2015)057

[22] J. Ellis, V. Sanz and T. You, *The effective standard model after LHC Run I*, *JHEP* **03** (2015) 157 [arXiv:1410.7703] [INSPIRE].

[23] R. Edezhath, *Dimension-6 operator constraints from boosted VBF Higgs*, arXiv:1501.00992 [INSPIRE].

[24] M. Gorbahn, J.M. No and V. Sanz, *Benchmarks for Higgs effective theory: extended Higgs sectors*, arXiv:1502.07352 [INSPIRE].

[25] Z. Han and W. Skiba, *Effective theory analysis of precision electroweak data*, *Phys. Rev.* **D 71** (2005) 075009 [hep-ph/0412166] [INSPIRE].

[26] M. Ciuchini, E. Franco, S. Mishima and L. Silvestrini, *Electroweak precision observables, new physics and the nature of a 126 GeV Higgs boson*, *JHEP* **08** (2013) 106 [arXiv:1306.4644] [INSPIRE].

[27] J. de Blas, *Electroweak limits on physics beyond the standard model*, *EPJ Web Conf.* **60** (2013) 19008 [arXiv:1307.6173] [INSPIRE].

[28] C.-Y. Chen, S. Dawson and C. Zhang, *Electroweak effective operators and Higgs physics*, *Phys. Rev.* **D 89** (2014) 015016 [arXiv:1311.3107] [INSPIRE].

[29] R. Alonso, E.E. Jenkins, A.V. Manohar and M. Trott, *Renormalization group evolution of the standard model dimension six operators III: gauge coupling dependence and phenomenology*, *JHEP* **04** (2014) 159 [arXiv:1312.2014] [INSPIRE].

[30] C. Englert et al., *Precision measurements of Higgs couplings: implications for new physics scales*, *J. Phys.* **G 41** (2014) 113001 [arXiv:1403.7191] [INSPIRE].

[31] M. Trott, *On the consistent use of constructed observables*, *JHEP* **02** (2015) 046 [arXiv:1409.7605] [INSPIRE].

[32] A. Falkowski and F. Riva, *Model-independent precision constraints on dimension-6 operators*, *JHEP* **02** (2015) 039 [arXiv:1411.0669] [INSPIRE].

[33] B. Henning, X. Lu and H. Murayama, *How to use the standard model effective field theory*, arXiv:1412.1837 [INSPIRE].

[34] J. de Blas, M. Chala, M. Pérez-Victoria and J. Santiago, *Observable effects of general new scalar particles*, *JHEP* **04** (2015) 078 [arXiv:1412.8480] [INSPIRE].

[35] L. Berthier and M. Trott, *Towards consistent electroweak precision data constraints in the SMEFT*, *JHEP* **05** (2015) 024 [arXiv:1502.02570] [INSPIRE].

[36] A. Efrati, A. Falkowski and Y. Soreq, *Electroweak constraints on flavorful effective theories*, *JHEP* **07** (2015) 018 [arXiv:1503.07872] [INSPIRE].

[37] B. Bhattacherjee, T. Modak, S.K. Patra and R. Sinha, *Probing Higgs couplings at LHC and beyond*, arXiv:1503.08924 [INSPIRE].

[38] CMS collaboration, *Constraints on the spin-parity and anomalous HVV couplings of the Higgs boson in proton collisions at 7 and 8 TeV*, *Phys. Rev.* **D 92** (2015) 012004 [arXiv:1411.3441] [INSPIRE].

[39] G. Amar et al., *Exploration of the tensor structure of the Higgs boson coupling to weak bosons in e^+e^- collisions*, *JHEP* **02** (2015) 128 [arXiv:1405.3957] [INSPIRE].

[40] S. Kumar and P. Poulose, *Influence of anomalous VVH and VVHH on determination of Higgs self couplings at ILC*, arXiv:1408.3563 [INSPIRE].

JHEP09(2015)057

[41] N. Craig, M. Farina, M. McCullough and M. Perelstein, *Precision Higgsstrahlung as a probe of new physics*, *JHEP* **03** (2015) 146 [arXiv:1411.0676] [INSPIRE].

[42] M. Beneke, D. Boito and Y.-M. Wang, *Signatures of anomalous Higgs couplings in angular asymmetries of $H \to Z\ell^+\ell^-$ and $e^+e^- \to HZ$*, arXiv:1411.3942 [INSPIRE].

[43] S. Kumar, P. Poulose and S. Sahoo, *Study of Higgs-gauge boson anomalous couplings through $e^-e^+ \to W^-W^+H$ at ILC*, *Phys. Rev.* **D 91** (2015) 073016 [arXiv:1501.03283] [INSPIRE].

[44] H.-Y. Ren, *New physics searches with Higgs-photon associated production at the Higgs factory*, arXiv:1503.08307 [INSPIRE].

[45] T. Plehn, D.L. Rainwater and D. Zeppenfeld, *Determining the structure of Higgs couplings at the LHC*, *Phys. Rev. Lett.* **88** (2002) 051801 [hep-ph/0105325] [INSPIRE].

[46] C. Bernaciak, M.S.A. Buschmann, A. Butter and T. Plehn, *Fox-Wolfram moments in Higgs physics*, *Phys. Rev.* **D 87** (2013) 073014 [arXiv:1212.4436] [INSPIRE].

[47] C. Bernaciak, B. Mellado, T. Plehn, P. Schichtel and X. Ruan, *Improving Higgs plus jets analyses through Fox-Wolfram moments*, *Phys. Rev.* **D 89** (2014) 053006 [arXiv:1311.5891] [INSPIRE].

[48] S.S. Biswal, R.M. Godbole, B. Mellado and S. Raychaudhuri, *Azimuthal angle probe of anomalous HWW couplings at a high energy ep collider*, *Phys. Rev. Lett.* **109** (2012) 261801 [arXiv:1203.6285] [INSPIRE].

[49] A. Djouadi, R.M. Godbole, B. Mellado and K. Mohan, *Probing the spin-parity of the Higgs boson via jet kinematics in vector boson fusion*, *Phys. Lett.* **B 723** (2013) 307 [arXiv:1301.4965] [INSPIRE].

[50] A. Djouadi, *Precision Higgs coupling measurements at the LHC through ratios of production cross sections*, *Eur. Phys. J.* **C 73** (2013) 2498 [arXiv:1208.3436] [INSPIRE].

[51] A. Djouadi and G. Moreau, *The couplings of the Higgs boson and its CP properties from fits of the signal strengths and their ratios at the $7+8$ TeV LHC*, *Eur. Phys. J.* **C 73** (2013) 2512 [arXiv:1303.6591] [INSPIRE].

[52] W. Buchmüller and D. Wyler, *Effective Lagrangian analysis of new interactions and flavor conservation*, *Nucl. Phys.* **B 268** (1986) 621 [INSPIRE].

[53] K. Hagiwara, R. Szalapski and D. Zeppenfeld, *Anomalous Higgs boson production and decay*, *Phys. Lett.* **B 318** (1993) 155 [hep-ph/9308347] [INSPIRE].

[54] M.C. Gonzalez-Garcia, *Anomalous Higgs couplings*, *Int. J. Mod. Phys.* **A 14** (1999) 3121 [hep-ph/9902321] [INSPIRE].

[55] B. Grzadkowski, M. Iskrzynski, M. Misiak and J. Rosiek, *Dimension-six terms in the standard model Lagrangian*, *JHEP* **10** (2010) 085 [arXiv:1008.4884] [INSPIRE].

[56] M.B. Einhorn and J. Wudka, *The bases of effective field theories*, *Nucl. Phys.* **B 876** (2013) 556 [arXiv:1307.0478] [INSPIRE].

[57] ATLAS collaboration, *Search for Higgs boson decays to a photon and a Z boson in pp collisions at $\sqrt{s} = 7$ and 8 TeV with the ATLAS detector*, *Phys. Lett.* **B 732** (2014) 8 [arXiv:1402.3051] [INSPIRE].

[58] CMS collaboration, *Search for a Higgs boson decaying into a Z and a photon in pp collisions at $\sqrt{s} = 7$ and 8 TeV*, *Phys. Lett.* **B 726** (2013) 587 [arXiv:1307.5515] [INSPIRE].

[59] LHC Higgs Cross section Working Group collaboration, J.R. Andersen et al., *Handbook of LHC Higgs cross sections: 3. Higgs properties*, arXiv:1307.1347 [INSPIRE].

JHEP09(2015)057

[60] CMS collaboration, *Precise determination of the mass of the Higgs boson and tests of compatibility of its couplings with the standard model predictions using proton collisions at 7 and 8 TeV*, *Eur. Phys. J.* **C 75** (2015) 212 [arXiv:1412.8662] [INSPIRE].

[61] ATLAS collaboration, *Measurements of the Higgs boson production and decay rates and coupling strengths using pp collision data at $\sqrt{s} = 7$ and 8 TeV in the ATLAS experiment*, ATLAS-CONF-2015-007, CERN, Geneva Switzerland (2015).

[62] A. Alloul, N.D. Christensen, C. Degrande, C. Duhr and B. Fuks, *FeynRules 2.0 — a complete toolbox for tree-level phenomenology*, *Comput. Phys. Commun.* **185** (2014) 2250 [arXiv:1310.1921] [INSPIRE].

[63] C. Degrande, C. Duhr, B. Fuks, D. Grellscheid, O. Mattelaer and T. Reiter, *UFO — the Universal FeynRules Output*, *Comput. Phys. Commun.* **183** (2012) 1201 [arXiv:1108.2040] [INSPIRE].

[64] J. Alwall et al., *The automated computation of tree-level and next-to-leading order differential cross sections and their matching to parton shower simulations*, *JHEP* **07** (2014) 079 [arXiv:1405.0301] [INSPIRE].

[65] T. Sjöstrand, S. Mrenna and P.Z. Skands, *PYTHIA 6.4 physics and manual*, *JHEP* **05** (2006) 026 [hep-ph/0603175] [INSPIRE].

[66] DELPHES 3 collaboration, J. de Favereau et al., *DELPHES 3, a modular framework for fast simulation of a generic collider experiment*, *JHEP* **02** (2014) 057 [arXiv:1307.6346] [INSPIRE].

[67] *LHC Higgs Cross Section Working Group webpage*, https://twiki.cern.ch/twiki/bin/view/LHCPhysics/CrossSections.

[68] ATLAS collaboration, *Projections for measurements of Higgs boson cross sections, branching ratios and coupling parameters with the ATLAS detector at a HL-LHC*, ATL-PHYS-PUB-2013-014, CERN, Geneva Switzerland (2013).

[69] ATLAS collaboration, *HL-LHC projections for signal and background yield measurements of the $H \to \gamma\gamma$ when the Higgs boson is produced in association with t quarks, W or Z bosons*, ATL-PHYS-PUB-2014-012, CERN, Geneva Switzerland (2014).

[70] ATLAS collaboration, *Measurement of Higgs boson production in the diphoton decay channel in pp collisions at center-of-mass energies of 7 and 8 TeV with the ATLAS detector*, *Phys. Rev.* **D 90** (2014) 112015 [arXiv:1408.7084] [INSPIRE].

[71] ATLAS collaboration, *Observation and measurement of Higgs boson decays to WW^* with the ATLAS detector*, *Phys. Rev.* **D 92** (2015) 012006 [arXiv:1412.2641] [INSPIRE].

[72] CMS collaboration, *Observation of the diphoton decay of the Higgs boson and measurement of its properties*, *Eur. Phys. J.* **C 74** (2014) 3076 [arXiv:1407.0558] [INSPIRE].

[73] CMS collaboration, *Precise determination of the mass of the Higgs boson and studies of the compatibility of its couplings with the standard model*, CMS-PAS-HIG-14-009, CERN, Geneva Switzerland (2014).

[74] I.W. Stewart and F.J. Tackmann, *Theory uncertainties for Higgs and other searches using jet bins*, *Phys. Rev.* **D 85** (2012) 034011 [arXiv:1107.2117] [INSPIRE].

[75] A. Kruse, A.S. Cornell, M. Kumar, B. Mellado and X. Ruan, *Probing the Higgs boson via vector boson fusion with single jet tagging at the LHC*, *Phys. Rev.* **D 91** (2015) 053009 [arXiv:1412.4710] [INSPIRE].

JHEP09(2015)057